Image processing of isotope yield in neutron-induced fission

Qufei Song ◉, Long Zhu, Boshuai Cai, Cenxi Yuan, and Jun Su ◉[*]
Sino-French Institute of Nuclear Engineering and Technology, Sun Yat-sen University, Zhuhai 519082, China

Hui Guo ◉
School of Nuclear Science and Engineering, Shanghai Jiao Tong University, Shanghai 200240, China

Background: Due to the complex multidimensional dependence, the prediction and evaluation of independent fission yield distributions have always been a challenge.

Purpose: Considering the complex multidimensional dependence and high missing rate of independent yield data, this study applies the tensor decomposition algorithm to the prediction of independent fission yields.

Methods: Tensor decomposition algorithm is a type of machine-learning algorithm with strong multidimensional structural dependencies capture ability, which is often used in the imputation of missing data in sparse tensors and has achieved great success in fields such as image processing and data mining. After constructing yield tensors with three dimensions for 851 fission products and filling the tensors with the independent yield data from the ENDF/B-VIII.0 database, the tensor decomposition algorithm is applied to predict the independent isotope yield in fission, which results the fission yield tensor decomposition (FYTD) model.

Results: The fission yields of ^{235}U and ^{239}Pu are set as missing values and then predicted. The mass distribution of ^{235}U fissions yield predicted by the FYTD model agrees well with the prediction of BNN + TALYS model and ENDF/B-VIII.0 data. Furthermore, the isotope yields in the fissions are also predicted. For fast neutron-induced fission of ^{239}Pu, 98% predictions of the isotope yields by the FYTD model agree with the ENDF/B-VIII.0 data within one order of magnitude. The fission yields of ^{238}Np, ^{243}Am, and ^{236}Np that do not exist in the ENDF/B-VIII.0 database are predicted and compared with those in the JEFF-3.3 database, as well as the experimental data. Good agreement demonstrates the predictive ability of the FYTD model for the target nucleus dependence. The scalability of the FYTD model over the incident neutron energy degrees of freedom is examined. After adding a set of 2 MeV neutron-induced ^{239}Pu fission yield data into the yield tensor, the 2 MeV neutron-induced fission yields of ^{235}U and ^{229}Th are predicted and consistent with the prediction of the GEF model and experimental data. Finally, the yields of the ratio of isomeric states and neutron excess of the products as a function of product charge number are also predicted and verified.

Conclusions: The FYTD model can capture the multidimensional dependence of the fission yield data and make reasonable predictions. This study proves the effectiveness of tensor decomposition algorithm in fission product yield study, and provides new ideas and tools for the evaluation and prediction of fission product yield data.

I. INTRODUCTION

The splitting of a heavy nucleus into two or more intermediate-mass nuclei is called fission. Although it has been more than 80 years since its discovery [1,2], the research on the fission is still a hot topic and challenge. On the one hand, the nuclear fission is an extremely complex process, which is the movement of the quantum multibody system composed of all nucleons in the nucleus in the multidimensional space. The exploration of its mechanism is very helpful to the development of nuclear physics fields such as nuclear structure, nuclear reaction and superheavy nuclear research [3–6].The nuclear fission also attracts attention in astrophysics and particle physics because it plays an important role in the formation of elements in the rapid neutron capture process (r-process) of nucleosynthesis and the production of reactor neutrinos [7,8]. On the other hand, the nuclear fission is also significant application fields. The huge energy released in the fission process makes fission play an important role in both energy and military fields. Neutrons and various radioisotopes produced by fission are used in various fields such as biology, chemistry, and medicine. Therefore, in order to make scientific use of fission, the research on the nuclear fission is widely concerned in the field of nuclear engineering and technology [9].

The fission product yield (FPY) is an important observable in the nuclear fission. Generally speaking, the nuclear fission is followed by the β decay of the unstable fragments. The FPY is divided into the independent and cumulative cases, which are distinguished by counting the products before and after the β decay. The independent fission product

———
[*]sujun3@mail.sysu.edu.cn

yield (IFPY) can reflect the information of fission process from the macro- and microperspectives, providing important observations for the research and modeling of fission processes [10]. However, experimental measurements of the IFPY are difficult and hence the available data are generally incomplete and have large uncertainties [11]. In major nuclear data libraries, such as ENDF/B [12], JEFF [13], and JENDL [14], complete evaluations of IFPY are not available for some certain actinides and only available for three neutron incident energy points (0.0253 eV, 0.5 MeV, and 14 MeV). Therefore, theoretical predictions of the IFPY are still necessary.

Due to the complexity of the quantum many-body problem and the nuclear force problem, the deep understanding and simulation of the fission process is still one of the most challenging tasks in nuclear physics [3,4]. Nowadays, the microscopic nuclear fission models, such as the time-dependent Hartree-Fock-Bogoliubov method [15] and the time-dependent generator coordinate method [16,17], have made important progress. The fission process can be regarded as a movement of Brownian particles walking on the multidimensional potential-energy surface. Various macroscopic-microscopic models based on the multidimensional potential-energy surface are also widely used in the calculation of the fission yield [18–21]. Some phenomenological methods, such as the multi-Gaussian semi-empirical formula [10,22], the Brosa model [23] and the GEF (general description of fission observables) model [24] are widely used and have achieved considerable success in evaluating fission yield data. The prediction of the GEF model is also referenced in the JEFF database to further improve the fission yield data in the database.

The traditional phenomenological models mainly rely on the least-squares adjustment of various parameters. They can describe the existing data in some regions well. But as fission modes evolve, the prediction capability of this type of models may be insufficient when the available experimental data are very sparse [25,26]. Recently, thanks to the powerful ability to learn from existing data and make predictions, the machine-learning algorithms have been used in various studies in the nuclear physics community. For example, the Bayesian neural network (BNN) algorithm has achieved certain success in prediction of nuclear mass [27,28], nuclear charge radius [29], spallation reaction product cross section [30,31], neutron and proton drip lines [32,33], etc. Likewise, various machine-learning algorithms have been applied to the study and prediction of fission yields. Lovell *et al.* used mixture density networks to learn parameters of Gaussian functions to predict fission product yields [34]. Tong *et al.* predicted the mass distribution of fission yield by combining KNN and GEF models [35]. Wang *et al.* predicted the mass distribution of fission yield by combining BNN and TALYS models and gave the confidence interval of the predicted value [26]. On the basis of this success, BNN model has been further developed and its accuracy has been further improved [36]. The charge distribution and isotopic distribution of fission yield can also be predicted by BNN model [37,38].

The tensor decomposition algorithm is a standard technique to capture the multidimensional structural dependence.

Compared with the traditional interpolation and fitting methods, the tensor decomposition algorithm has a strong ability to extract the information hidden in the original data, making it possible to impute the sparse tensor, which makes it widely used in image processing, data mining, and other fields [39–41]. Considering the complex multidimensional dependence and high missing rate of independent yield data, this study applies the tensor decomposition algorithm to the prediction of independent fission yields, and establishes the fission yield tensor decomposition (FYTD) model. The paper is organized as follows: In Sec. II, the establishment of FYTD model is described. In Sec. III, FYTD model will be applied to multiple yield prediction for verification. Finally, Sec. IV presents conclusions and perspectives for future studies.

II. THEORETICAL FRAMEWORK

A. Tensorization of fission product yield

The neutron-induced fission is briefly introduced by taking a typical ^{235}U(n, f) reaction as an example:

$$^{235}_{92}\text{U} + n \longrightarrow ^{236}_{92}\text{U}^* \longrightarrow ^{92}_{36}\text{Kr} + ^{141}_{56}\text{Ba} + 3n. \qquad (1)$$
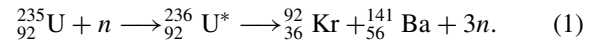
A specific target nucleus, such as ^{235}U, can be represented by its number of protons Z_t and number of neutrons N_t. The target nucleus forms an excited composite nucleus after the neutron incident with energy E_n. After fission of composite nucleus, two primary fission products, one light and one heavy, are produced and several prompt neutrons are released. Thus, the neutron-induced fission yield of a given isotope with number of protons Z_p and number of neutrons N_p depends on the neutron incident energy and target nuclei. In addition, a considerable part of the fission products are not in the ground state but in the isomeric state. To distinguish these products, the fission product state (FPS) needs to be considered.

Therefore, when tensorizing the neutron-induced fission product yield data, six dimensions can be considered, including E_n, Z_t, N_t, Z_p, N_p, and FPS. Among six dimensions, the dimensions related to the target nucleus and product are discrete, and only the neutron incident energy E_n is continuous. Therefore, E_n is discretized into thermal neutron (0.0253 eV), fast neutron (0.5 MeV), and high-energy neutron (14 MeV).

Nowadays, due to the difficulty of IFPY experimental measurement and the lack of existing data, this yield tensor will have a very high degree of missingness. Imputation of such sparse tensors has always been a challenge. Similar scenes also appear in image processing in the computer field. A color image can be thought of as a multidimensional tensor containing information about the pixel location dimension, as well as the pixel color dimension. To deal with color images with high missing rate and high signal-to-noise ratio, tensor decomposition algorithms are widely used [39–41]. Taking the left image in Fig. 1 as an example, 70% of the pixels in this image are missing. We tensorized the image and applied the BGCP algorithm to capture the multidimensional information of the remaining pixels. Finally, as shown in the middle image of Fig. 1, tensor decomposition can effectively impute the missing pixels. From the naked eye, the details of the image are not well restored compared with the original image, but the overall trend of the images are consistent.

FIG. 1. Image imputation by tensor decomposition algorithm.

The tensor decomposition algorithm for image processing is helpful for predicting the fission yield. However, six dimensions are included when tensorizing the fission yields, including E_n, Z_t, N_t, Z_p, N_p, and FPS. In the ENDF/B-VIII.0 database, 851 products are concerned, containing 710 fission products at the ground state, 133 kinds of $M1$ isomeric state and 8 kinds of $M2$ isomeric state. The three-dimensional (3D) yield tensors with dimensions Z_t, $N_t - Z_t$, and E_n are constructed for each product nuclide. Then, there are 851 3D tensors. The range of the 3D tensors is chosen as $Z_t = 90$–96, $N_t - Z_t = 47$–54, and $E_n = 0.0253$ eV, 0.5 MeV, 14 MeV. By filling these 3D tensors with the ENDF/B-VIII.0 data of 45 fission reactions for 24 target nuclei of ^{227,229,232}Th, ^{231}Pa, ^{232,233,234,236,237,238}U, ^{237,238}Np, $^{238-242}$Pu, ^{241,243}Am, and $^{242-246}$Cm, the missing rate of the tensor is about 73%, which is similar to that of the missing image showing in Fig. 1.

Now, let Y_{ijk}^p represent the yield of fission product p, where i, j, k represents Z_t, $N_t - Z_t$, and E_n respectively. For example, $Y_{3,5,1}^{I135}$ is entry with $i = 3(Z_t = 92)$, $j = 5(N_t - Z_t = 51)$ and $k = 1$ ($E_n = 0.0253$ eV), which represents the ^{135}I yield in 0.0253 eV neutron-induced fission of ^{235}U. For data existing in the ENDF/B-VIII.0 database, the value of Y_{ijk}^p is filled with ENDF/B-VIII.0 data. For reactions not found in the ENDF/B-VIII.0 database, the value is missing. The magnitude of the independent yield is very small, even up to 10^{-18}. Therefore, it is necessary to fill the tensor with the natural logarithm of the yield, in case this data are too small for numerical calculation. This approach works well for products with big variation, allowing the algorithm to capture magnitude changes in yield well. But for products with small yield variation, the difference is even smaller after logarithmization, and it is difficult for the algorithm to capture their difference. Therefore, to solve this problem, we analyzed the degree of dispersion of 851 product yield data under different fission reactions. In this study the degree of dispersion is defined as the standard deviation of the natural logarithm values of the existing yield data:

$$\sigma_{\text{yield}}^p = \sqrt{\sum_{i=1}^{I} \sum_{j=1}^{J} \sum_{k=1}^{K} b_{ijk} \frac{\left[\ln\left(Y_{ijk}^p\right) - \overline{\ln\left(Y^p\right)} \right]^2}{\sum_{i=1}^{I} \sum_{j=1}^{J} \sum_{k=1}^{K} b_{ijk}}}, \quad (2)$$

where b_{ijk} is one for the existing yield data and zero for the missing yield data, $\overline{\ln(Y^p)}$ is the average of natural logarithms of all existing ENDF/B-VIII.0 data. If $\sigma_{\text{yield}}^p > 1$, its magnitude varies greatly, and the yield value is logarithmized during filling; otherwise, the yield value remains linear.

At this point, we obtain 851 3D tensors, in which about 73% of the elements are unmeasured. With the help of the tensor decomposition algorithm [40], the values of unmeasured elements in each tensor are completed, so as to obtain a yield tensor without missing values. Since the tensor decomposition of each product is independent of each other, the superscript p representing the fission product is omitted in the following derivation.

B. Bayesian Gaussian CANDECOMP/PARAFAC tensor decomposition

A detailed introduction to the Bayesian Gaussian CANDECOMP/PARAFAC (BGCP) algorithm can be found in Ref. [40]. Here is a brief introduction to the application of BGCP in this study. In the derivation, bold symbols represent tensors, matrices or vectors, while nonbold symbols represent numbers. It is assumed that the uncertainty of each existing yield data Y_{ijk} follows an independent Gaussian distribution,

$$Y_{ijk} \sim \mathcal{N}\left(\hat{Y}_{ijk}, \tau_\epsilon^{-1}\right), \quad (3)$$

where τ_ϵ is the precision, which is a universal parameter for all elements. As described in Ref. [40], in order to improve the robustness of the model, a flexible conjugate Γ prior is used for the precision instead of a fixed value, and its distribution will be updated with the training process. In this study, the original uncertainty of the training data is not considered. In the further study, the ability to consider the original error may be realized by improving the distribution of τ_ϵ. In real-world applications the expectation of yield $\hat{Y}_{ijk}$ is unknown and replaced with the estimated yield, which is the entry of the estimated tensor $\hat{\mathcal{Y}}$. The CP decomposition is applied to calculate the estimation $\hat{\mathcal{Y}}$:

$$\hat{\mathcal{Y}} = \sum_{n=1}^{r} \boldsymbol{z}^{(n)} \circ \boldsymbol{d}^{(n)} \circ \boldsymbol{e}^{(n)}, \quad (4)$$

where $z^{(n)} \in \mathbb{R}^I$, $d^{(n)} \in \mathbb{R}^J$, and $e^{(n)} \in \mathbb{R}^K$ are respectively the n-th column vector of the factor matrices $Z \in \mathbb{R}^{I \times r}$, $D \in \mathbb{R}^{J \times r}$, and $E \in \mathbb{R}^{K \times r}$. In the tensor decomposition algorithm, a three-dimensional tensor will be decomposed into three two-dimensional matrices. Z, D, and E are these three two-dimensional matrices, which contain information in three dimensions. For example, Z contains the characteristic information of fission yield changing with the target charge number.

The symbol $\circ$ represents the outer product, and thus $z^{(n)} \circ d^{(n)} \circ e^{(n)}$ is a rank-one tensor. With this formulation, the CP decomposition of a tensor can be considered as sum of r rank-one component tensors, and r is called the CP rank of tensor $\hat{\mathcal{Y}}$. The larger the CP rank, the more information the factor matrix can contain, and the stronger the learning ability of the algorithm, but it is also more likely to lead to over-fitting. To prevent the over-fitting, $r = 5$ is used in this study.

The ith row vector of the factor matrix Z is denoted $z_i \in \mathbb{R}^r$. Similarly, $d_j \in \mathbb{R}^r$ and $e_k \in \mathbb{R}^r$ are respectively the jth row vector of D and the kth row vector of E. The prior distribution of row vector is the multivariate Gaussian:

$$z_i \sim \mathcal{N}\left[\mu_i^{(z)}, \left(\Lambda_i^{(z)}\right)^{-1}\right], \quad (5)$$

where the hyper-parameter $\mu^{(z)} \in \mathbb{R}^r$ expresses the expectation, and $\Lambda^{(z)} \in \mathbb{R}^{r \times r}$ indicates the width of the distribution. The likelihood function can be written as

$$\mathcal{L}(Y_{ijk} \mid z_i, d_j, e_k, \tau_\epsilon) \propto \exp\left\{-\frac{\tau_\epsilon}{2}[Y_{ijk} - (z_i)^T(d_j \circledast e_k)]^2\right\}, \quad (6)$$

where $\circledast$ is the Hadamard product.

Then, according to Bayesian theorem, the posterior distribution of z_i after observing Y_{ijk} is

$$\begin{aligned}
&\mathcal{L}(z_i \mid Y_{ijk}, d_j, e_k, \tau_\varepsilon) \\
&\quad \propto \mathcal{L}(Y_{ijk} \mid z_i, d_j, e_k, \tau_\varepsilon) \Pr(z_i) \\
&\quad \propto \exp\left\{-\frac{\tau_\varepsilon}{2}[Y_{ijk} - (z_i)^T(d_j \circledast e_k)]^2\right\} \\
&\qquad \times \mathcal{N}\left[\mu_i^{(z)}, \left(\Lambda_i^{(z)}\right)^{-1}\right]. \quad (7)
\end{aligned}$$

Then the posterior values of the hyper-parameters $\mu^{(z)}$ and $\Lambda^{(z)}$ are given as

$$\begin{aligned}
&\widehat{\Lambda}_i^{(z)} = \Lambda_i^{(z)} + \Delta\Lambda_i^{(z)}, \quad \Delta\Lambda_i^{(z)} = \tau_\varepsilon(d_j \circledast e_k)(d_j \circledast e_k)^T, \\
&\hat{\mu}_i^{(z)} = \mu_i^{(z)} + \Delta\mu_i^{(z)}, \quad \Delta\mu_i^{(z)} \\
&\quad = \left(\widehat{\Lambda}_i^{(z)}\right)^{-1}(d_j \circledast e_k)\tau_\varepsilon\left[Y_{ijk} - (d_j \circledast e_k)^T\mu_i^{(z)}\right]. \quad (8)
\end{aligned}$$

The contributions to the hyper-parameter of each existing yield data are equivalent to each other, and the likelihood function of all existing yield data is

$$\begin{aligned}
&\mathcal{L}(\mathcal{Y} \mid Z, D, E, \tau_\epsilon) \\
&\quad \propto \prod_{i=1}^I \prod_{j=1}^J \prod_{k=1}^K (\tau_\epsilon)^{1/2} \exp\left[-\frac{\tau_\epsilon}{2} b_{ijk}(Y_{ijk} - \hat{Y}_{ijk})^2\right], \quad (9)
\end{aligned}$$

where b_{ijk} is one for the existing yield data and zero for the missing yield data. Placing a conjugate Γ prior to the precision τ_ϵ,

$$\tau_\epsilon \sim \Gamma(a_0, b_0). \quad (10)$$

The posterior values of the hyperparameters a_0 and b_0 are given as

$$\begin{aligned}
\hat{a}_0 &= \frac{1}{2}\sum_{i=1}^I\sum_{j=1}^J\sum_{k=1}^K b_{ijk} + a_0, \\
\hat{b}_0 &= \frac{1}{2}\sum_{i=1}^I\sum_{j=1}^J\sum_{k=1}^K (Y_{ijk} - \hat{Y}_{ijk})^2 + b_0. \quad (11)
\end{aligned}$$

Based on Eq. (11), each existing yield data contributes to the increase of $\frac{1}{2}$ in $\hat{a}_0$, and $\frac{1}{2}(Y_{ijk} - \hat{Y}_{ijk})^2$ in $\hat{b}_0$.

In Fig. 2, the above method is illustrated and an example is given. In brief, for a specific fission product, we denote its yields in different fission reactions by $\hat{\mathcal{Y}}$. According to the CP decomposition, the tensor $\hat{\mathcal{Y}}$ is expressed as sum of r rank-one component tensors. The rank-one component tensors are the outer products of the column vector of factor matrices Z, D, and E. The prior distributions of the factor matrices are assumed to be multivariate Gaussians. With the existing observed yield data, the posterior values of the factor matrices and their distributions can be calculated using Bayesian inference and iteration. Taking the prediction of ^{236}Np fission yield induced by 0.5 MeV neutrons as an example, the information captured by the algorithm comes from the existing data on the same dimension, the same Z_t data (^{237}Np and ^{238}Np data), the same $N_t - Z_t$ data (^{234}U and ^{238}Pu yield data), and all yield data at the same energy (0.5 MeV). Finally, the predicted fission yield is reconstituted with the sum of rank-one component tensors.

Without considering ternary fission, two fragments are produced in each fission event, so the sum of all fission product yields should also be two. However, after tensor reconstruction, the sum of the yields obtained is not strictly two due to the precision of numerical calculation, and the yield of completion is always slightly smaller, such as 1.96, 1.98, etc. Therefore, it is necessary to perform a certain physical correction on the value. If a detailed normalization work is carried out, a variety of constraints and conservations should be considered. There are other important normalization methods that conserve charge, mass, and charge parity [42]. In this paper, this complex normalization method is not fully realized. We refer to this method and make some simplification. The mass of the compound nucleus minus the number of prompt neutrons is divided by two, and this value is used as the standard to judge whether the fission products belong to light nuclei or heavy nuclei, and the yields of light nuclei and heavy nuclei are normalized to one, respectively. After normalization, the predicted yield data are finally obtained.

III. RESULTS AND DISCUSSIONS

To quantitatively evaluate the prediction of the FYTD model, the root mean square error (RMSE) and χ_N^2 are used to measure the deviation between prediction and the ENDF/B-VIII.0 data. For the convenience of presentation, ENDF/B-VIII.0 is abbreviated as ENDF/B in the following
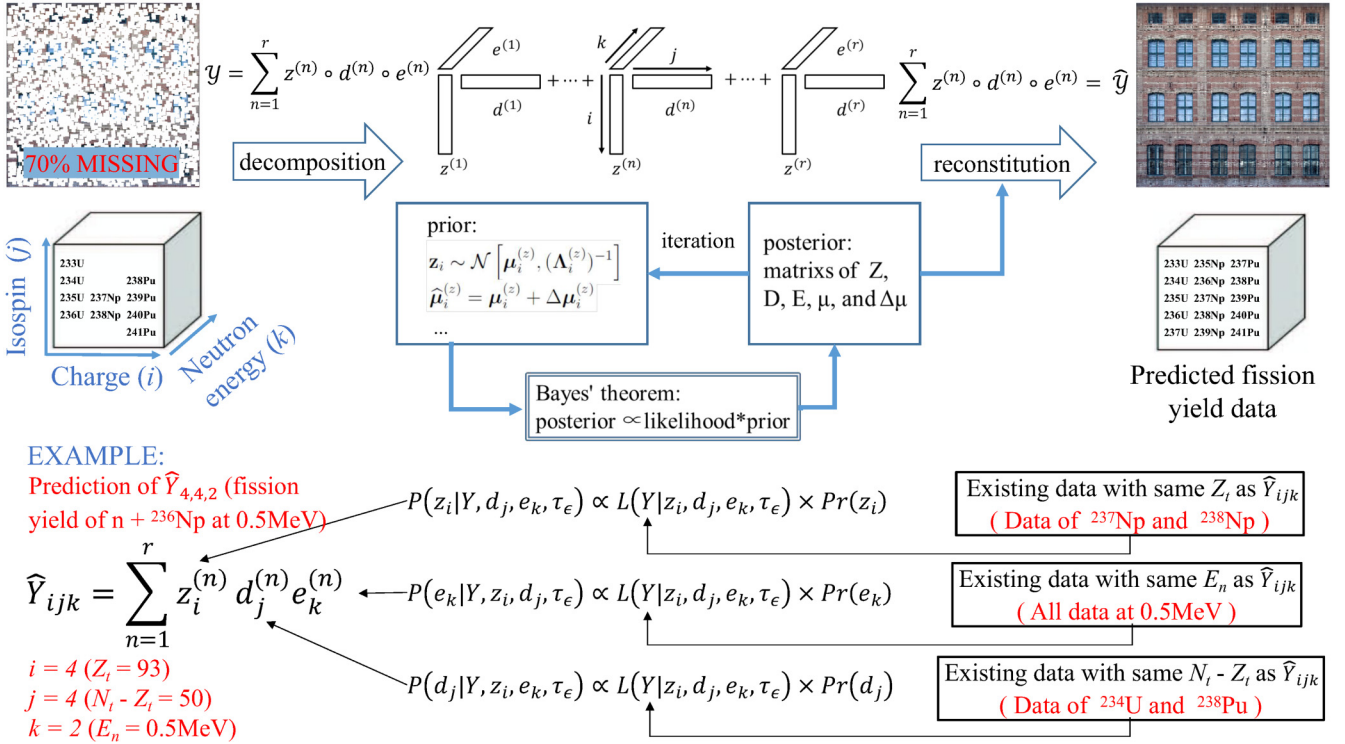
FIG. 2. Model framework presentation and example.

text and figures. For a fission reaction, the RMSE is calculated by evaluating the deviation of the predicted results of its 851 products from the ENDF/B:

$$\text{RMSE} = \sqrt{\frac{1}{N} \sum_{p=1}^{N} [\log_{10}(\widehat{Y}^p) - \log_{10}(Y^p)]^2}, \qquad (12)$$

where $N = 851$, $\widehat{Y}^p$ represents the FYTD model prediction of the yield of the pth product, and Y^p represents the corresponding ENDF/B data.

Considering most current fission yield prediction studies and experimental measurements mainly focus on the mass distribution of the product, in order to compare with other models and data, as defined in Ref. [26], use χ_N^2 to measure the deviation of the predicted value of the mass distribution from the ENDF/B data:

$$\chi_N^2 = \frac{1}{N} \sum_{p=1}^{N} (\widehat{Y}^p - Y^p)^2. \qquad (13)$$

Here $N = 107$, which means the range of statistics is A = 66–172 for a total of 107 mass points.

The evaluation of RMSE and χ_N^2 have different emphases. In calculation of RMSE, the magnitude difference between the predicted value of each product and the ENDF/B data is considered, which can globally evaluate the accuracy of magnitude prediction. Therefore it does not ignore the contribution of some products with small yield values. In contrast, χ_N^2 focuses more on evaluating the accuracy of peak area predictions.

A. ENDF/B-VIII.0 data prediction

In this part, the ENDF/B yield data for each fission reaction are sequentially removed and predicted by FYTD model to systematically analyze the learning and prediction ability of FYTD model. Table I shows the RMSE of the FYTD model when predicting each fission reaction. In general, it can be seen that, after removing the data to be predicted, the more remaining data in the learning set with the same dimension as the data to be predicted, the smaller the RMSE. For example, the RMSE of the prediction data for U, Pu, and Cm are mostly small, because even if the learning data of a fission reaction is removed, there are still many existing data in the same dimension that can capture information during prediction. For ^{229}Th and ^{232}Th, after removing their data from the learning set, there are few existing data that can be referenced when predicting them, resulting in a high RMSE. It can be found that the largest RMSE occurs at ^{227}Th and ^{232}U. This is because after the data of ^{227}Th was removed, the data of $j = 1$ ($N_t - Z_t = 47$) does not exist in the learning set at all. Therefore, when making predictions, it is completely impossible to capture the information of this dimension, resulting in unreliable predictions and extremely large RMSE.

This phenomenon reflects a shortcoming of the tensor decomposition algorithm, which is caused by the characteristics of tensors. Different from BNN and other models, variables in FYTD model are not continuous, but discrete. The size of these variables depends on their position in the tensor. It should be noted that $j = 1$ is defined as $N_t - Z_t = 47$ because all data with $N_t - Z_t = 47$ are placed in the position of $j = 1$. If these data are removed, then $j = 1$ is no longer meaningful

TABLE I. The RMSE of prediction by the FYTD model comparing with the ENDF/B-VIII.0 data. The blank values mean there are not evaluation data in the ENDF/B-VIII.0 database.

RMSE	0.0253 eV	0.5 MeV	14 MeV
^{227}Th	2.034		
^{229}Th	1.095		
^{232}Th		0.942	0.866
^{231}Pa		1.005	
^{232}U	1.874		
^{233}U	0.598	0.473	0.411
^{234}U		0.659	0.244
^{235}U	0.622	0.552	0.260
^{236}U		0.391	0.271
^{237}U		0.419	
^{238}U		0.712	0.683
^{237}Np	0.466	0.612	0.622
^{238}Np		0.607	
^{238}Pu		0.768	
^{239}Pu	0.429	0.281	0.390
^{240}Pu	0.284	0.326	0.554
^{241}Pu	0.652	0.424	
^{242}Pu	0.451	0.482	1.170
^{241}Am	0.560	0.495	0.498
^{243}Am		0.638	
^{242}Cm		0.839	
^{243}Cm	0.683	0.521	
^{244}Cm		0.443	
^{245}Cm	0.779		
^{246}Cm		0.637	

and cannot represent any variable. Therefore, in imputation of tensor decomposition algorithm, at least one datum is needed on each dimension to make the dimension meaningful. Only when this requirement is met can each dimension of the tensor be well defined, and the tensor decomposition algorithm can correctly capture the multidimensional dependence. Predictions lacking dimensional information are unreliable and should be avoided when predicting using FYTD model. And in all following predictions, all calculations will avoid this problem.

B. ^{235}U and ^{239}Pu fission yield prediction

In this part, all ^{235}U or ^{239}Pu yield under the three energy points are set as missing values, and the FYTD model is used to reproduce the ^{235}U or ^{239}Pu yield data. The predictions will be verified by comparing with ENDF/B-VIII.0 data and the predictions of the TALYS model and the BNN + TALYS model taken from Ref. [26]. The BNN + TALYS model predictions are quite satisfactory regarding the distribution positions and energy dependencies of fission yields. The prediction can be improved by reinforcement learning. In addition to giving the mean value of the prediction, BNN models can also give the associated confidence interval of the prediction value, which can reasonably estimate the evaluation uncertainty. The uncertainty of the final prediction results mainly comes from two parts, one is the uncertainty of the original training data, and the other is the uncertainty given
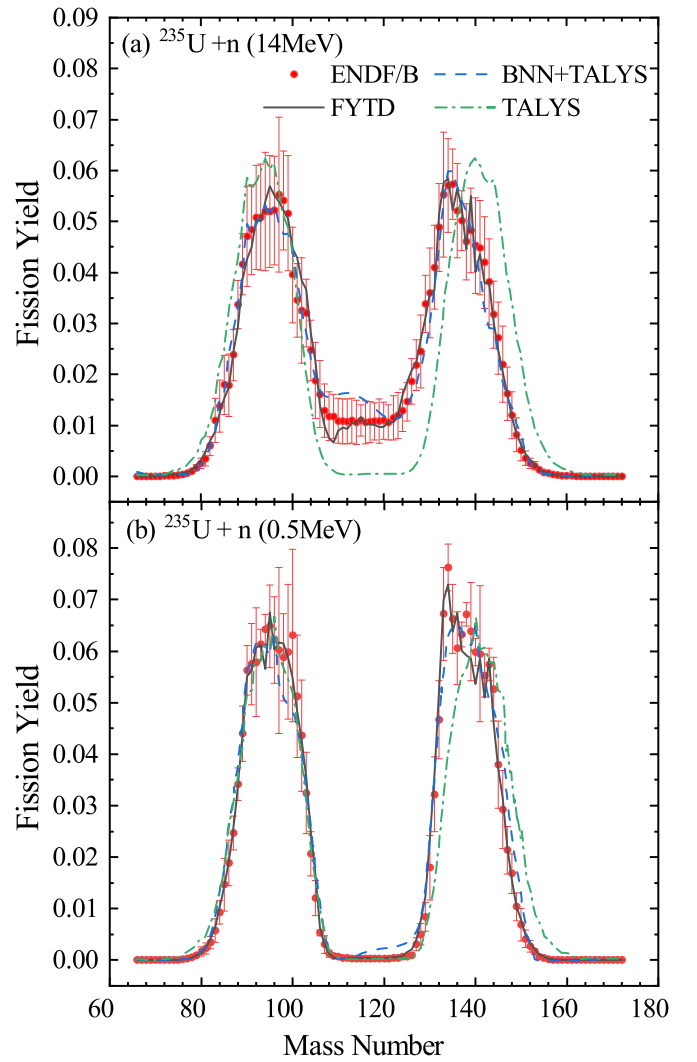

FIG. 3. ^{235}U fission yield mass distribution predicted by various models and corresponding ENDF/B-VIII.0 data (red dot), at neutron incident energies of (a) 14 MeV and (b) 0.5 MeV. The black solid curves, blue dashed curves, and dash-dotted curves represent the predictions of FYTD, BNN + TALYS, and TALYS models, respectively. BNN + TALYS and TALYS predictions are taken from Ref. [26].

by the algorithm. In Ref. [26], the uncertainty given by the algorithm is considered in BNN model. In further study in Ref. [38], the BNN model is improved and both the two kinds of uncertainty can be considered. At present, the FYTD model can only give the uncertainty of the algorithm, without considering the uncertainty of the original data, thus it is compared with the results in Ref. [26]. In addition, JENDL-4.0 data were used for model training in Ref. [26], and this paper uses the ENDF/B-VIII.0 data. However, the fission yield data in JENDL database actually refer to that in ENDF/B database, the fission yield data in these two database are almost the same. Both the prediction by the BNN + TALYS model and the FYTD model are made when all ^{235}U yield data in the learning set are removed. Thus, it is suitable to compare with the prediction by the FYTD model.

TABLE II. The validation errors χ_N^2 of various models. Errors for TALYS, BNN-40, and BNN-40 + TALYS are taken from Ref. [26].

Models	Validation $\chi_N^2(10^{-5})$
TALYS [43]	8.334
BNN-40 [26]	1.640
BNN-40 + TALYS [26]	1.134
FYTD	0.701

Figure 3 shows the predicted mass distribution of the products in ^{235}U fission at 14 MeV and 0.5 MeV. The χ_N^2 of predictions are shown in Table II. It can be seen from Fig. 3 that the TALYS model has a deviation from the ENDF/B data at the heavy nucleus peak and did not predict the neutron energy dependence of valley yields well. After combining the trained BNN algorithm, the BNN + TALYS model can correct these deviations. In general, predictions of BNN + TALYS model and FYTD model are basically consistent with the ENDF/B data, but both have some deviations in the valley. This result proves that, when all ^{235}U yield data in the learning set are removed, the FYTD model can effectively capture information from other heavy nucleus yield data and predict the ^{235}U yield data. At the same time, it can also capture the neutron energy dependence information of yield data and predict the variation trend of yield with neutron energy.

Figure 3 is the comparison of mean value predictions, the uncertainty of predictions is not compared. The uncertainty of the prediction of FYTD model is not shown in the figure because it is too small to be visible. This is understandable to some extent, because the FYTD model can refer to many existing data in this case. When there are less existing data available for prediction, the FYTD model will give bigger uncertainties, as shown in Fig. 7. Different from the relatively

similar mean value predictions, the uncertainty predictions of BNN + TALYS model and FYTD model differ greatly. In Ref. [26], BNN + TALYS model can give relatively large uncertainty. Considering that neither model takes into account the uncertainty of the original data, the reason for this difference is unknown. Therefore, we will further discuss this issue when the original data uncertainty can be considered in the FYTD model, and then the comparison with prediction in Ref. [38] will be more meaningful.

Furthermore, the isotope yields in the fissions are also predicted. To more comprehensively show the difference between the predicted isotopic yields and the ENDF/B-VIII.0 data of 851 fission products, Fig. 4 shows the logarithmic error distribution of the fast neutron-induced fission product yield of ^{239}Pu and the RMSE of the predicted results. A dotted line with zero error is marked in the two figures. The closer the dot is to the line, the smaller the error. The RMSE of the prediction result at this time is 0.395, which is little higher than the 0.281 in Table I. This is understandable, because the learning set of this prediction result removes all the data of all three energy points of ^{239}Pu, while the test in Table I only removes the data of one energy point. It can be seen from Fig. 4(a) that the greater the yield value of the product, the higher the accuracy of the prediction. This confirms that the method of constructing tensors with partial logarithmic and partial linear coordinates can make nuclide prediction with large yield more accurate. Figure 4(b) shows the count of errors of different sizes. It can be seen that the logarithmic error of 98% isotopes is within ±1. that is, the difference between the predicted yield and ENDF/B data is within one order of magnitude. And for 88% nuclides, the difference between the predicted yield and ENDF/B data is within 0.5 orders of magnitude. However, it can be seen from Fig. 4(a) that ^{239}Pu fast neutron-induced fission yield data spans 16 orders of magnitude from 10^{-18}
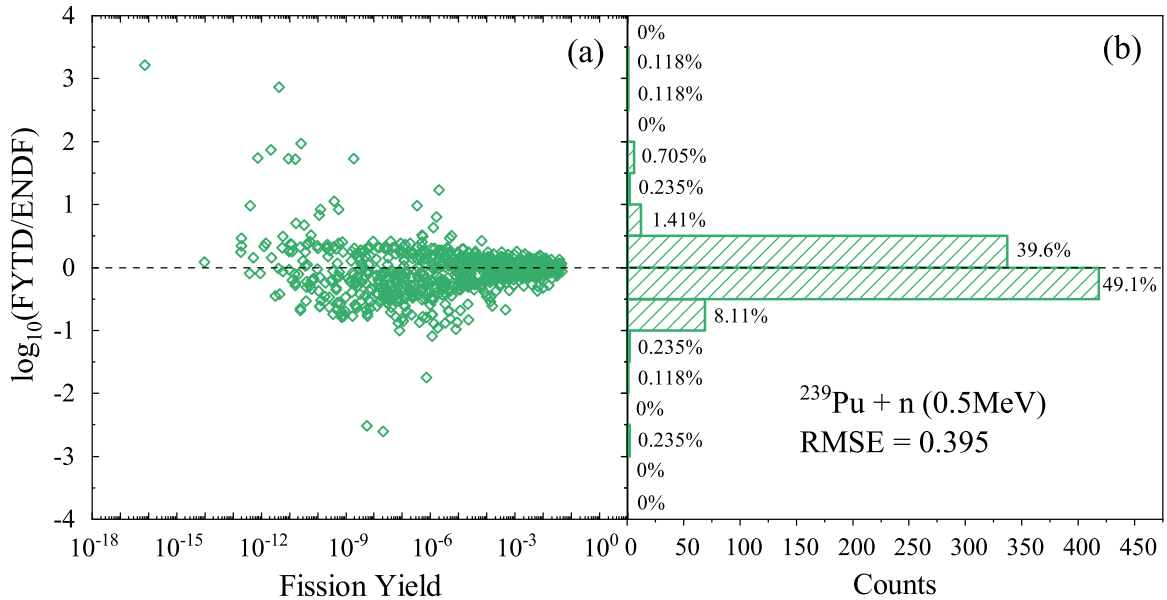

FIG. 4. Denary logarithm of the ratio of FYTD prediction to ENDF/B-VIII.0 data (logarithmic error) for 0.5 MeV neutron-induced ^{239}Pu fission. Panel (a) is the distribution of errors and panel (b) is the count of errors of different sizes. Each dot represents a product, the ordinate is the prediction error of the product, and the abscissa is the yield of the product.
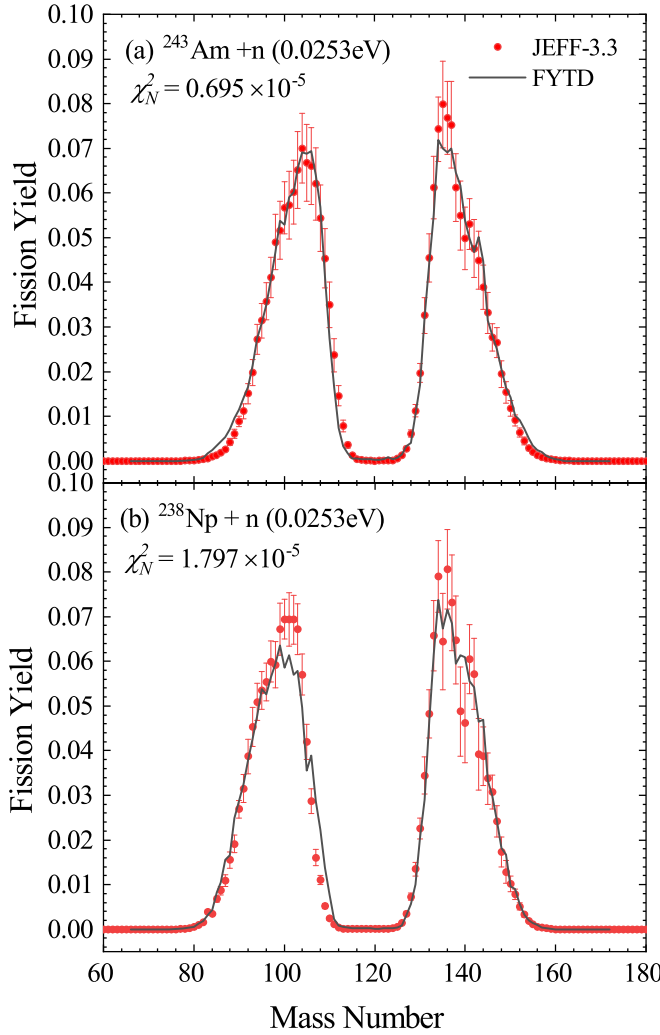
FIG. 5. Fission yield mass distribution predicted by FYTD model (black solid curves) and corresponding JEFF-3.3 data (red dots), for (a) ^{243}Am $+n$ at 0.0253 eV and (b) ^{238}Np $+n$ at 0.0253 eV.

to 10^{-3}, this prediction of isotope distribution by the FYTD model is relatively satisfactory.

C. ^{238}Np, ^{243}Am, and ^{236}Np fission yield prediction

After several verification, it is proved that the FYTD model has good learning and prediction ability for ENDF/B data. In this part, we maintain the previous ENDF/B training set unchanged and predict the data that do not exist in the ENDF/B database. To verify whether the predicted results are reliable, the predicted yield data will be compared with the JEFF database and experimental data.

Taking ^{243}Am and ^{238}Np as examples, their fission yield data under thermal neutrons is missing in the ENDF/B-VIII.0 database, but they exist in the JEFF-3.3 database. The predicted fission yield will be compared with the data in JEFF-3.3. Figure 5 shows the comparison of yield mass distribution. It can be seen from Fig. 5(a) that the prediction of ^{243}Am by the FYTD model is basically within the error range of JEFF data, the χ_N^2 is 0.659×10^{-5}. Only at the edge A = 80–85,
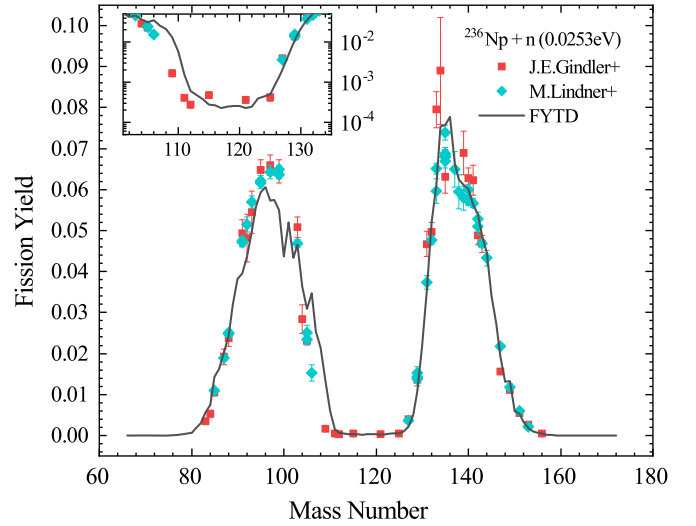

FIG. 6. Fission yield mass distribution of ^{236}Np $+n$ at 0.0253 eV predicted by FYTD model (black solid curves) and two sets of corresponding experimental data (red and green dots) from Refs. [44,45]. The inset on the upper left shows the valley areas in logarithmic scale.

there is a little deviation between the prediction results and the JEFF data. For prediction of ^{238}Np in Fig. 5(b), there is a certain deviation at the light nucleus peak. Therefore, the χ_N^2 is bigger, reaching 1.797×10^{-5}.

From the above two comparisons, it can be seen that the prediction of the FYTD model for the yield data of ^{243}Am and ^{238}Np under thermal neutrons are consistent with the JEFF data, but this is based on the existing data. As can be seen from Table I, ^{243}Am and ^{238}Np have no data under thermal neutrons but under fast neutrons in ENDF/B database. It is relatively easy for the FYTD model to predict the data of a target nucleus at one energy points when the data at other energy point is known. However, the yield data of some target nuclei are very scarce, such as ^{236}Np. Its independent yield data are missing in both ENDF/B and JEFF databases, and there are only a few experimental measurement data of chain yield. To predict the yield data of ^{236}Np, it is necessary to capture information from other target nuclei, which tests the model's ability to learn and predict the dependence of target nucleus.

Figure 6 show the mass distribution of fission products in thermal fission of ^{236}Np measured by the two experimental groups and the corresponding predictions by the FYTD model. The panel on the upper left is added to show the valley areas in logarithmic scale. It can be seen that the predictions by the FYTD model at heavy nucleus peak agree with the two sets of experimental data, and there is a slight deviation near $A = 100$ at light nucleus peak. As for the valley value, the predicted magnitude is consistent with the experimental data. This result proves the ability of FYTD model to learn and predict the target nucleus dependence of FPY.

D. Prediction of 2 MeV neutron-induced fission yield

The above prediction of this neutron energy dependence is limited in three energy points. To verify the scalability of the FYTD model over the incident neutron energy degrees of
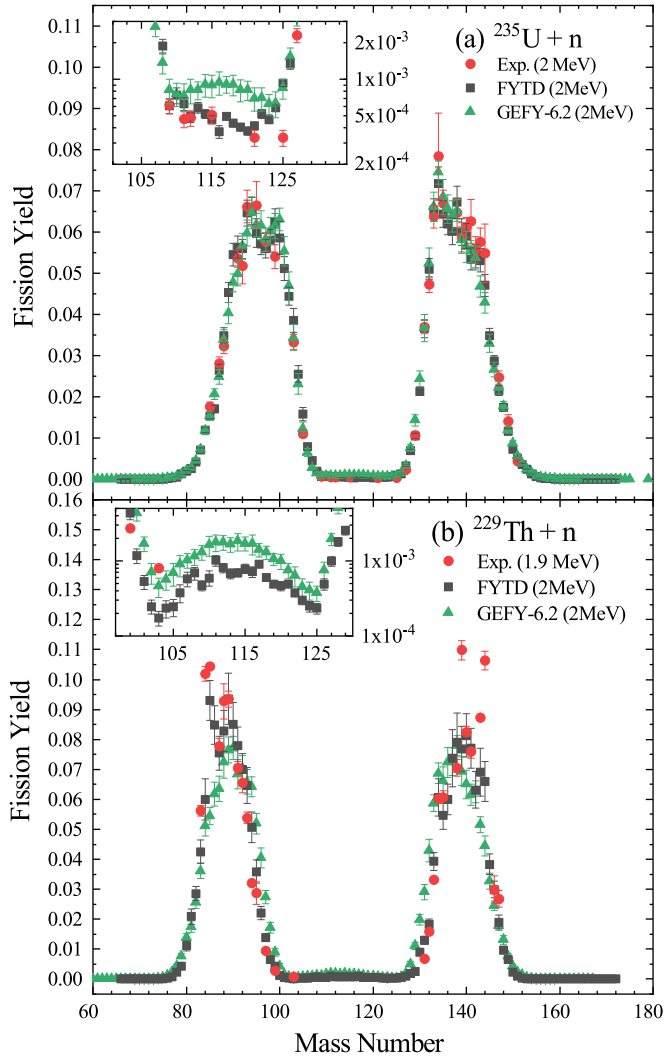
FIG. 7. Fission yield mass distribution for (a) ^{235}U and (b) ^{229}Th at 2 MeV predicted by FYTD model (black dots), GEF model (green dots), and corresponding experimental data (red dots) from Refs. [46,47]. The insets show the valley areas in logarithmic scale.

FIG. 8. Neutron excess as a function of product charge number for ^{235}U $+n$ fission at different energies, in which the 2 MeV results are predicted by the FYTD model. Spherical shell $Z = 50$, $N = 82$ and deformed shells $Z = 44$, $N = 64$ are marked by dashed lines.

freedom and predict FPY data under 2 MeV, the only FPY data under 2 MeV (^{239}Pu $+n$ at 2 MeV) in ENDF/B-VIII.0 database is included in the training set. Then the FYTD model can predict the 2 MeV FPY data of the remaining heavy nuclei in the tensor. The reliability of this prediction is verified by comparison with experimental data and the predictions of the GEF model. The data of the GEF model comes from the database GEFY-6.2.

Figure 7 shows the mass distribution of the products in ^{235}U and ^{229}Th fissions at 2 MeV. It can be seen from Fig. 7(a) that both predictions by the FYTD and GEF models agree well with experimental data in the peak area. In the valley area shown in the inset, the prediction by the FYTD model is slightly closer to the experimental data than that of GEF model. For predictions for ^{229}Th in Fig. 7(b), no completely strict experimental data for ^{229}Th at 2 MeV are published. The experimental data at 1.9 MeV were used for comparison. According to energy dependence, it can be simply speculated
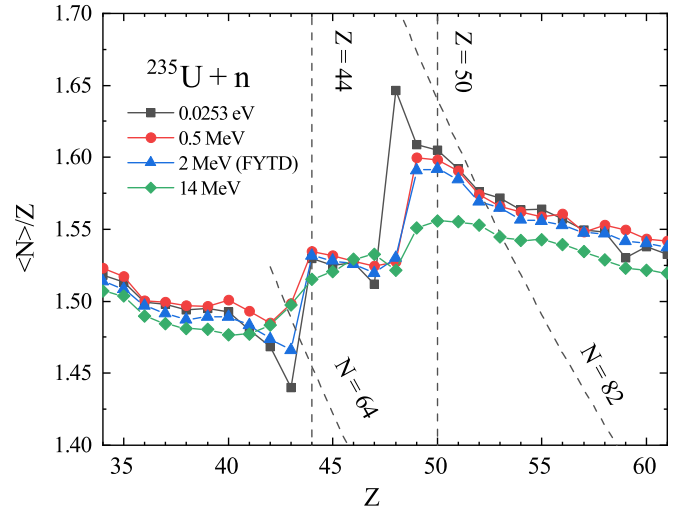
that the data at 1.9 MeV should be slightly higher than the data at 2 MeV in the peak area, and lower in the valley area. The peak predicted by the FYTD model is just slightly lower than the experimental value and higher than that predicted by the GEF model. Overall, the prediction of FYTD model is basically consistent with the prediction of GEF model and experimental data.

It is worth noting that, since there is only one existing 2 MeV datum that can be referred to during the prediction, the prediction uncertainty given by the FYTD model is much higher than that in the previous prediction, it can be clearly observed in the Fig. 7 now. In addition, the uncertainty of ^{229}Th is greater than that of ^{235}U, because the existing Th data is far less than U. In general, the uncertainty given by the FYTD model at present follows a rule. The less existing data to learn, the greater the uncertainty of the prediction.

Then neutron excess and proportion of isomeric states is calculated to further verify the prediction. Figure 8 shows the neutron excess of ^{235}U fission products induced by neutrons of different energies. The data of 2 MeV are the prediction by the FYTD model, and the rest are for ENDF/B data. The positions of some shells are marked in the figure. The definition of neutron excess is referred to the Ref. [10] and is defined as the ratio of the average neutron number to the proton number of the product. This quantity can reflect the neutron proton composition of the fission product and the influence of shell effect on fission. From the data at 0.0253 eV, 0.5 MeV, and 14 MeV in the figure, it can be observed that the neutron proton composition of the product is greatly affected by the shells of $Z = 50$, $N = 82$ and $Z = 44$, $N = 64$. However, with the increase of neutron incident energy, the excitation energy of compound nucleus increases, and the curve gradually flattens. This is because the increase of excitation energy will hinder the influence of shell effect, and the increase of valley area in yield mass distribution is also caused by this reason. It can be seen from the figure that the predicted data under
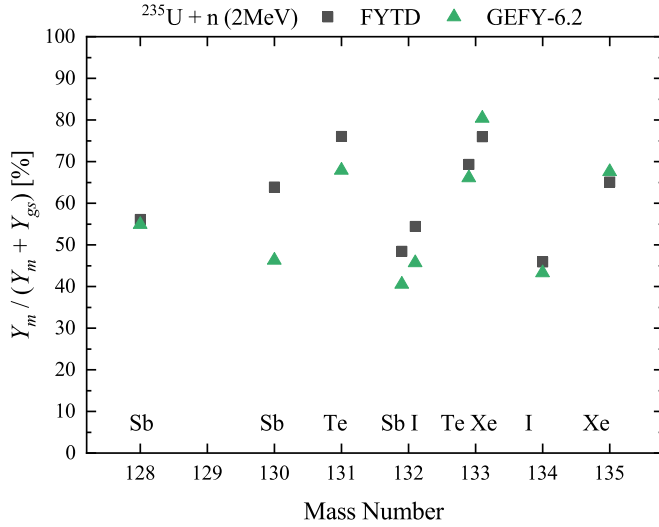
FIG. 9. Isomeric ratios predicted by FYTD model (black dots) and GEF model (green dots) for several fission products from ^{235}U $+n$ at 2 MeV.

2 MeV neutron incidence generally conforms to this law. In most areas, the predictions are between 0.5 and 14 MeV data, and only deviate at $Z = 43$. This verification further proved that FYTD model learn and predict the impact of excitation energy on yield.

In the FYTD model, the isomeric states of products can be considered, and the corresponding data can be learned and predicted. Figure 9 shows the proportion of isomeric states for ^{128}Sb, ^{130}Sb, ^{131}Te, ^{132}Sb, ^{132}I, ^{133}Te, ^{133}Xe, ^{134}I, and ^{135}Xe produced in fission. It can be seen that, except for ^{130}Sb, the predictions by the FYTD model are consistent with those by the GEF model. The above comparison further proved the ability of FYTD model to learn and predict the multidimensional dependence of FPY. Predictions for fission at 2 MeV also proves that the FYTD model is not only applicative at 0.0253 eV, 0.5 MeV, and 14 MeV, but also extend to other neutron energy with the help of data for one target nucleus.

IV. CONCLUSION

This study applied the tensor decomposition algorithm to the prediction of independent fission product yields. A fission yield tensor decomposition model was established and applied to a variety of yield predictions for verification.

The fission yields of ^{235}U and ^{239}Pu are set as missing values and then predicted. The predicted fission yields of ^{235}U under fast neutron and high-energy neutron incident are compared with prediction of TALYS and BNN + TALYS models. The FYTD model can learn and predict the neutron energy dependence of the yield data, the prediction of FYTD model agrees well with the prediction of BNN + TALYS model and ENDF/B-VIII.0 data. The data for ^{239}Pu fission under fast neutron incident spans 16 orders of magnitude from 10^{-3} to 10^{-18}. Comparison between the prediction and ENDF/B-VIII.0 data for 851 fission products shows that 98% of them agree with each other within one order of magnitude, and 88% within 0.5 orders of magnitude.

By comparing the predictions with the data of ^{238}Np and ^{243}Am in the JEFF-3.3 database, as well as the experimental data of ^{236}Np, the predictive ability of the model for the target nucleus dependence of the yield data is demonstrated. The scalability of the yield tensor decomposition model over the incident neutron energy degrees of freedom is examined. After adding a set of 2 MeV neutron-induced ^{239}Pu fission yield data into the yield tensor, the 2 MeV neutron-induced fission yields of ^{235}U and ^{229}Th are predicted. The prediction of the FYTD model is basically consistent with the prediction of the GEF model and experimental data. At the same time, the prediction and verification of the isomeric states ratio and neutrons excess of the products further prove the prediction ability of the FYTD model.

The multiple rounds of comparative verification show that the FYTD model can capture the complex multidimensional dependence of fission yields and make reasonable predictions. This study proves the effectiveness of tensor decomposition algorithm in FPY study, and provides new ideas and tools for the evaluation and prediction of FPY data. However, there are still some unsolved problems. First, the FYTD model can only give the uncertainty of the algorithm, and does not consider the uncertainty of the original data at present. Second, FYTD model handles discrete dimensions such as Z and N-Z well, but has defects in predicting continuous energy dimensions. The continuous change of FPY data with energy cannot be predicted, and the prediction of new energy points depends on existing data. Finally, the model currently contains fewer physical images and constraints. These problems need to be solved in a future study. In addition, the predictions and evaluations of this study are based on the ENDF/B-VIII.0 database. In the future we will conduct evaluations based on the EXFOR database.

[1] O. Hahn and F. Strassmann, Naturwissenschaften **27**, 11 (1939).
[2] L. Meitner and O. R. Frisch, Nature (London) **143**, 239 (1939).
[3] N. Schunck and L. Robledo, Rep. Prog. Phys. **79**, 116301 (2016).

[4] M. Bender, R. Bernard, G. Bertsch, S. Chiba, J. Dobaczewski, N. Dubray, S. A. Giuliani, K. Hagino, D. Lacroix, Z. Li *et al.*, J. Phys. G **47**, 113002 (2020).

[5] J. Hamilton, S. Hofmann, and Y. Oganessian, Annu. Rev. Nucl. Part. Sci. **63**, 383 (2013).

[6] J. C. Pei, W. Nazarewicz, J. A. Sheikh, and A. K. Kerman, Phys. Rev. Lett. **102**, 192501 (2009).

[7] M. Eichler, A. Arcones, A. Kelic, O. Korobkin, K. Langanke, T. Marketin, G. Martínez-Pinedo, I. Panov, T. Rauscher, S. Rosswog, C. Winteler, N. T. Zinner, and F.-K. Thielemann, Astrophys. J. Lett. **808**, 30 (2015).

[8] T. A. Mueller, D. Lhuillier, M. Fallot, A. Letourneau, S. Cormon, M. Fechner, L. Giot, T. Lasserre, J. Martino, G. Mention, A. Porta, and F. Yermia, Phys. Rev. C **83**, 054615 (2011).

[9] L. A. Bernstein, D. A. Brown, A. J. Koning, B. T. Rearden, C. E. Romano, A. A. Sonzogni, A. S. Voyles, and W. Younes, Annu. Rev. Nucl. Part. Sci. **69**, 109 (2019).

[10] D. Ramos, M. Caamaño, F. Farget, C. Rodríguez-Tajes, L. Audouin, J. Benlliure, E. Casarejos, E. Clement, D. Cortina, O. Delaune, X. Derkx, A. Dijon, D. Doré, B. Fernández-Domínguez, G. de France, A. Heinz, B. Jacquot, C. Paradela, M. Rejmund, T. Roger *et al.*, Phys. Rev. C **99**, 024615 (2019).

[11] H. O. Denschlag, Nucl. Sci. Eng. (La Grange Park, IL, U.S.) **94**, 337 (1986).

[12] D. Brown, M. Chadwick, R. Capote, A. Kahler, A. Trkov, M. Herman, A. Sonzogni, Y. Danon, A. Carlson, M. Dunn, D. Smith, G. Hale, G. Arbanas, R. Arcilla, C. Bates, B. Beck, B. Becker, F. Brown, R. Casperson, J. Conlin *et al.*, Nucl. Data Sheets **148**, 1 (2018).

[13] Joint Evaluated Fission and Fusion (JEFF) Nuclear Data Library, https://www.oecd-nea.org/dbdata/jeff/.

[14] K. Shibata, O. Iwamoto, T. Nakagawa, N. Iwamoto, A. Ichihara, S. Kunieda, S. Chiba, K. Furutaka, N. Otuka, T. Ohsawa, T. Murata, H. Matsunobu, A. Zukeran, S. Kamada, and J.-i. Katakura, J. Nucl. Sci. Technol. (Abingdon, U.K.) **48**, 1 (2011).

[15] A. Bulgac, P. Magierski, K. J. Roche, and I. Stetcu, Phys. Rev. Lett. **116**, 122504 (2016).

[16] D. Regnier, N. Dubray, N. Schunck, and M. Verrière, Phys. Rev. C **93**, 054611 (2016).

[17] W. Younes, D. M. Gogny, and J.-F. Berger, *A Microscopic Theory of Fission Dynamics Based on the Generator Coordinate Method*, Lecture Notes in Physics Vol. 950 (Springer International, Cham, 2019).

[18] J. Randrup and P. Möller, Phys. Rev. Lett. **106**, 132503 (2011).

[19] J. Randrup, P. Möller, and A. J. Sierk, Phys. Rev. C **84**, 034613 (2011).

[20] K. Pomorski, F. A. Ivanyuk, and B. Nerlo-Pomorska, Eur. Phys. J. A **53**, 59 (2017).

[21] L.-L. Liu, X.-Z. Wu, Y.-J. Chen, C.-W. Shen, Z.-X. Li, and Z.-G. Ge, Phys. Rev. C **99**, 044614 (2019).

[22] Z.-X. Fang, M. Yu, Y.-G. Huang, J.-B. Chen, J. Su, and L. Zhu, Nucl. Sci. Tech. **32**, 72 (2021).

[23] U. Brosa, S. Grossmann, and A. Müller, Phys. Rep. **197**, 167 (1990).

[24] K.-H. Schmidt, B. Jurado, C. Amouroux, and C. Schmitt, Nucl. Data Sheets **131**, 107 (2016).

[25] K.-H. Schmidt and B. Jurado, Rep. Prog. Phys. **81**, 106301 (2018).

[26] Z.-A. Wang, J. Pei, Y. Liu, and Y. Qiang, Phys. Rev. Lett. **123**, 122501 (2019).

[27] Z. Niu and H. Liang, Phys. Lett. B **778**, 48 (2018).

[28] R. Utama, J. Piekarewicz, and H. B. Prosper, Phys. Rev. C **93**, 014311 (2016).

[29] R. Utama, W.-C. Chen, and J. Piekarewicz, J. Phys. G **43**, 114002 (2016).

[30] C.-W. Ma, D. Peng, H.-L. Wei, Z.-M. Niu, Y.-T. Wang, and R. Wada, Chin. Phys. C **44**, 014104 (2020).

[31] Q.-F. Song, L. Zhu, and J. Su, Chin. Phys. C **46**, 074108 (2022).

[32] L. Neufcourt, Y. Cao, W. Nazarewicz, E. Olsen, and F. Viens, Phys. Rev. Lett. **122**, 062502 (2019).

[33] L. Neufcourt, Y. Cao, S. Giuliani, W. Nazarewicz, E. Olsen, and O. B. Tarasov, Phys. Rev. C **101**, 014319 (2020).

[34] A. E. Lovell, A. T. Mohan, and P. Talou, J. Phys. G **47**, 114001 (2020).

[35] L. Tong, R. He, and S. Yan, Phys. Rev. C **104**, 064617 (2021).

[36] Z.-A. Wang and J. Pei, Phys. Rev. C **104**, 064608 (2021).

[37] C. Y. Qiao, J. C. Pei, Z. A. Wang, Y. Qiang, Y. J. Chen, N. C. Shu, and Z. G. Ge, Phys. Rev. C **103**, 034621 (2021).

[38] Z. A. Wang, J. C. Pei, Y. J. Chen, C. Y. Qiao, F. R. Xu, Z. G. Ge, and N. C. Shu, Phys. Rev. C **106**, L021304 (2022).

[39] J. Liu, P. Musialski, P. Wonka, and J. Ye, IEEE Trans. Pattern Anal. Mach. Intell. **35**, 208 (2013).

[40] X. Chen, Z. He, and L. Sun, Transp. Res. Part C: Emerg. Technol. **98**, 73 (2019).

[41] X. Chen, Z. Han, Y. Wang, Q. Zhao, D. Meng, L. Lin, and Y. Tang, IEEE Trans. Neural Netw. Learning Syst. **29**, 5380 (2018).

[42] E. F. Matthews, L. A. Bernstein, and W. Younes, At. Data Nucl. Data Tables **140**, 101441 (2021).

[43] A. J. Koning and D. Rochman, Nucl. Data Sheets, **113**, 2841 (2012).

[44] M. Lindner and D. W. Seegmiller, Radiochim. Acta **49**, 1 (1990).

[45] J. Gindler, L. Glendenin, E. Krapp, S. Fernandez, K. Flynn, and D. Henderson, J. Inorg. Nucl. Chem. **43**, 445 (1981).

[46] L. E. Glendenin, J. E. Gindler, D. J. Henderson, and J. W. Meadows, Phys. Rev. C **24**, 2600 (1981).

[47] C. Agarwal, A. Goswami, P. C. Kalsi, S. Singh, A. Mhatre, and A. Ramaswami, J. Radioanal. Nucl. Chem. **275**, 445 (2008).